Hyperthermal Oxidation of Si(100)2×1 Surfaces: Effect of Growth Temperature

ARTICLE *in* THE JOURNAL OF PHYSICAL CHEMISTRY C · APRIL 2012

Impact Factor: 4.77 · DOI: 10.1021/jp300506g

4 AUTHORS, INCLUDING:

Umedjon Khalilov
University of Antwerp
17 PUBLICATIONS **145** CITATIONS
SEE PROFILE

Adri C.T. van Duin
Pennsylvania State University
361 PUBLICATIONS **8,150** CITATIONS
SEE PROFILE

Erik C. Neyts
University of Antwerp
110 PUBLICATIONS **1,621** CITATIONS
SEE PROFILE

THE JOURNAL OF PHYSICAL CHEMISTRY C

Article

pubs.acs.org/JPCC

Hyperthermal Oxidation of Si(100)2×1 Surfaces: Effect of Growth Temperature

U. Khalilov,*[,†] G. Pourtois,[†,‡] A. C. T. van Duin,[§] and E. C. Neyts[†]

[†]Department of Chemistry, PLASMANT Research Group, University of Antwerp, Universiteitsplein 1, B-2610 Wilrijk-Antwerp, Belgium

[‡]IMEC, Kapeldreef 75, B-3001 Leuven, Belgium

[§]Department of Mechanical and Nuclear Engineering, Penn State University, University Park, Pennsylvania 16801, United States

ABSTRACT: Using reactive molecular dynamics simulations based on the ReaxFF potential, we studied the growth mechanism of ultrathin silica (SiO_2) layers during hyperthermal oxidation as a function of temperature in the range 100−1300 K. Oxidation of Si(100){2 × 1} surfaces by both atomic and molecular oxygen was investigated for hyperthermal impact energies in the range of 1 to 5 eV. Two different growth mechanisms are found, corresponding to a low temperature oxidation and a high temperature one. The transition temperature between these mechanisms is estimated to be about 700 K. Also, the initial step of the Si oxidation process is analyzed in detail. Where possible, we validated our results with experimental and ab initio data, and good agreement was obtained. This study is important for the fabrication of silica-based devices in the micro- and nanoelectronics industry and, more specifically, for the fabrication of metal−oxide semiconductor devices.

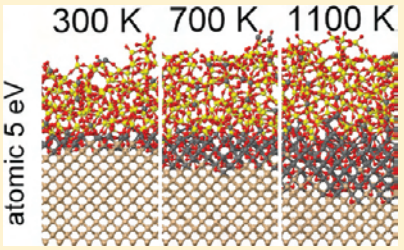

INTRODUCTION

Recently, interest in hyperthermal oxidation of the Si surface as an alternative to thermal oxidation has been rapidly increasing, especially for semiconductor applications. Indeed, it was discovered that the reaction of hyperthermal oxygen species (O, O_2) with a Si surface has unique properties compared to ordinary high temperature oxidation, i.e., a very thin oxide film can be formed even at room temperature.[1−6] Furthermore, since silicon oxide is commonly employed as a protective transparent coating in spacecraft applications, the study of the surface reaction of energetic oxygen species as dominant components of the low-Earth orbital (LEO) is also important.[7,8] As a result, many investigations were recently devoted to this topic, in order to elucidate the fundamental aspects of the hyperthermal impact and oxidation process.[1−10]

Reaction and diffusion of oxygen atoms and molecules during thermal oxidation have been previously analyzed both by experimental and theoretical means.[11−20] However, for hyperthermal oxidation, such studies are still rare. Although numerous studies have elucidated the overall oxidation behavior,[1−5] various aspects, such as direct oxidation or the effect of the growth temperature, are still poorly understood. Also, there are still many open questions regarding the growth mechanism in the initial oxidation stage as a function of temperature, which is significantly different from the mechanism in the thermal oxidation case.

According to the generally adopted Deal−Grove model[21] for thermal wet and dry oxidation, silicon oxide films grow via diffusion of oxidants, i.e., oxygen atoms or molecules to the SiO_2|Si interface and by reaction of these oxygen species with silicon at the interface. Unfortunately, it is well-known that the model fails to describe the oxidation kinetics of thin films (<100 Å).[22,23] Furthermore, the concept is only applicable for thermal oxidation at high temperature and low pressure. For thermal oxidation of thin films, several models, which are considered as modifications of the original Deal−Grove idea, have already been presented [e.g., refs 24 and 25]. However, the onset of hyperthermal Si oxidation cannot be described by these models. For example, Cerofolini et al.[25] presented a model for the oxidation kinetics in air at room temperature, based on the Elovich equation,[26] which is generally applied to chemisorption kinetics.[27,28] However, the kinetic model fails in two situations for describing the hyperthermal oxidation: (a) there is no solution of the equation for the formation of substoichiometric oxides in the case $\theta(0) = 0$, that is, when there is no pre-existing oxide layer on the Si surface prior to oxidation; and (b) there are no suitable parameters for describing the direct oxidation, i.e., energetic oxygen species directly oxidizing the Si subsurface layers. Another extension of the Deal−Grove idea is the Massoud−Plummer−Irene extension.[24] They reported data for the oxidation rate for layers with a thickness between about 20 Å and 500 Å. However, there is little or no experimental data extending continuously downward from 20 Å on. The formation of an ultrathin SiO_2 layer (with a thickness less than 20 Å) cannot be explained by this model. Such thin layers can, however, be obtained by hyperthermal oxidation of Si at room temperature.[6]

Some other models, such as the so-called reactive layer model,[29] have also been presented. According to this model, silicon atoms diffuse through the thin reactive layer and react

Received: January 16, 2012
Revised: March 15, 2012
Published: March 26, 2012

   dx.doi.org/10.1021/jp300506g | J. Phys. Chem. C 2012, 116, 8649−8656

with oxygen on the top of this layer, forming the SiO_2 phase. Unfortunately, little experimental evidence has been reported to support this idea.[22] The atomistic mechanism of Si emitting from the $SiSiO_2$ interface was reported,[30] which was in fairly good agreement with experimental results corresponding to layer-by-layer Si oxidation theory.[19] However, the oxide growth mechanism is not described well by this theory.[25] Furthermore, the outward diffusion of Si has not been investigated yet for hyperthermal oxidation.

Indeed, the growth mechanism of silicon dioxide in the initial stage of hyperthermal oxidation has not yet been properly analyzed, and investigations at the atomic scale may further elucidate the growth mechanism. Although our previous work[6] was devoted to understanding the oxidation process of the Si(100) surface by energetic oxygen species (i.e., O atoms and O_2 molecules with initial energies from 1 to 5 eV) at room temperature on the atomic scale, the oxide formation and growth mechanism at higher temperatures in hyperthermal oxidation is still unclear. Therefore, we carried out reactive molecular dynamics (MD) calculations in order to investigate the growth mechanism of new oxide layers during hyperthermal oxidation (i.e., initial kinetic energies in the range 1−5 eV) of the (2 × 1) reconstructed Si(100) surface in a wide temperature range (100−1300 K). The Si(100) surface was chosen, as this is the most important surface facet for metal−oxide semiconductor device fabrication.

COMPUTATIONAL DETAILS

Interatomic Potential. The growth process of SiO_2 during hyperthermal oxidation of Si at the atomic scale is studied by reactive MD simulations. Forces on the atoms are derived from the Reactive Force Field (ReaxFF) potential, developed by van Duin et al.[31] The ReaxFF potential uses the bond order/bond distance relationship formally introduced by Abell.[32] Over-coordination and undercoordination energy penalties are used to enforce the correct bond order. The total system energy is the sum of several partial energy terms related to lone pairs, undercoordination, overcoordination, valence and torsion angles, conjugation, and hydrogen bonding, as well as van der Waals and Coulomb interactions. The ReaxFF potential has been shown not only to describe covalent bonds but also ionic bonds and the whole range of intermediate interactions. Charge distributions are calculated based on geometry and connectivity using the electronegativity equalization method (EEM).[33] A detailed description of the force field can be found elsewhere.[34−36] In this work, we use the force field parameters employed by Buehler et al.[36] for crack propagation in silicon. The force field was extensively trained against Si and SiO_2 phases, but Si suboxide components were not taken into account. A force field evaluation against suboxide stabilities and oxygen migration barriers is warranted to validate the current results. Nevertheless, wherever comparison with experiment or ab initio data is available, the current force field reproduces these data faithfully. Currently, the ReaxFF potential is being successfully used for describing numerous elements and their compounds, including hydrocarbons, silicon/silicon oxide,[37,38] metals and metal-catalyzed reactions,[39,40] metal oxides,[41] metal hydrides,[42] and others.

Simulation Method. Prior to oxygen impact, eight Si(100) {2 × 1} surfaces were prepared as follows. First, the surfaces are equilibrated at 100 K, 300 K, 500 K, 700 K, 900 K, 1100 K, 1200 K, and 1300 K using the Berendsen heat bath (NVT dynamics)[43] for 20 ps with a damping constant of 0.1 ps. Then, the obtained structures are relaxed in the microcanonical ensemble (NVE dynamics) for 10 ps. Energetic oxygen impacts are performed as follows. The incident particle (oxygen atom or oxygen molecule) is positioned at a z position of 10 Å above the uppermost Si atom of the crystal. The $\{x, y\}$ coordinates of the incident particles are chosen randomly. In the case of molecular oxygen, the O_2 molecule is rotated randomly prior to impact. The impinging particle is directed normal to the surface, corresponding to laser detonation experiments.[1,7] Every impact is followed for 3 ps. The initial kinetic energies of the oxygen species (O, O_2) were set to 1 eV, 3 eV, and 5 eV. In total, 48 different cases were investigated for the oxidation process, i.e., 3 different impact energies for both atomic and molecular oxygen at the 8 different growth temperatures, as mentioned above. Each case was run for 1024 consecutive impacts, corresponding to a growth thickness of 32 monolayers (ML).

RESULTS AND DISCUSSION

Hyperthermal Oxidation Process at Various Growth Temperatures. Figure 1 shows the distribution of the formed oxygenated silicon layers for various growth temperatures after 32 monolayers (ML) of oxygen impacts, both for molecular (M) and atomic (A) oxygen impacts at 1 and 5 eV. In our calculations, 1 ML equals 32 atoms. The gray and red atoms represent silicon and oxygen atoms, respectively. As can been seen in the figure, the oxidized silicon can be divided in two parts: an interface region and pure silica. Our previous results on hyperthermal oxidation at room temperature showed that also the silica (SiO_2) region (yellow region in Figure 1) can be divided in two sections: a surface region and a bulk region. The interface region, which is located between the crystalline Si and

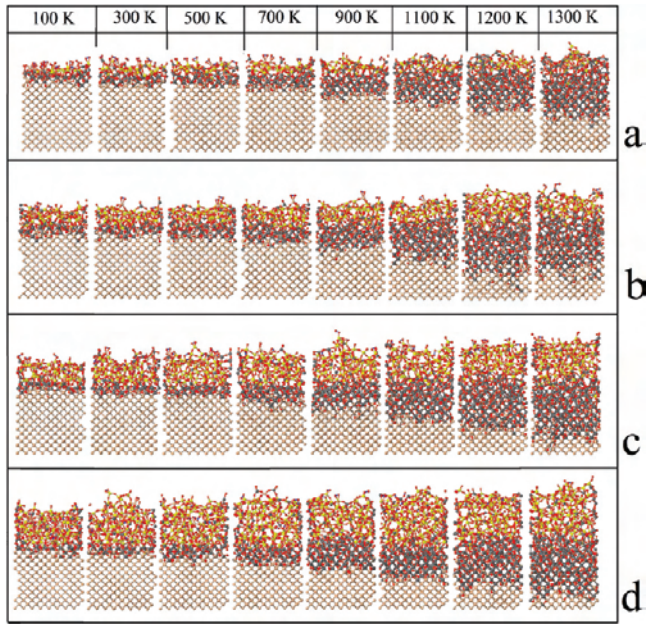

Figure 1. Illustration of the temperature effect on the oxidation of silicon after 32 monolayers (ML) of oxygen impacts, by oxygen molecules at E_0 = 1 eV (M1) and E_0 = 5 eV (M5) and by oxygen atoms at E_0 = 1 eV (A1) and E_0 = 5 eV (A5). Note that 1 ML corresponds to 32 atoms. Here, the Si crystal (Si^0), interface (Si^{1+}, Si^{2+}, and Si^{3+}), silica (Si^{4+}), and oxygen atoms are colored light gray, dark gray, yellow, and red, respectively.

dx.doi.org/10.1021/jp300506g | J. Phys. Chem. C 2012, 116, 8649−8656

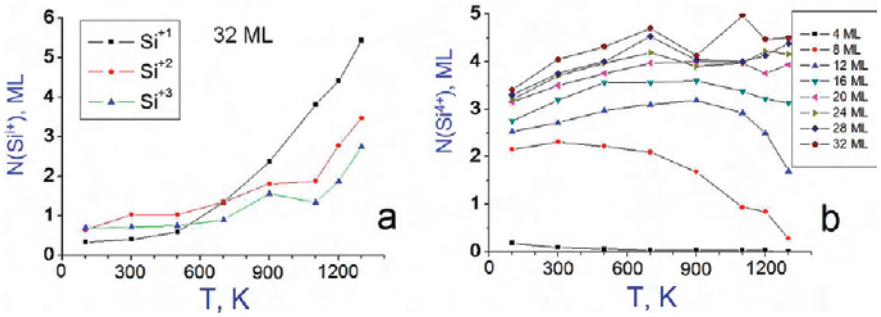

Figure 2. (a) Analysis of the interface region by the total number of Si^{1+}, Si^{2+}, and Si^{3+} suboxide components (expressed in ML) as obtained after 32 ML of atomic oxygen impacts for a kinetic energy E_0 = 5 eV, as a function of oxidation temperature. (b) Total number of Si^{4+}, expressed in ML, in the interface region, as a function of oxidation temperature, after a specific number of impacts, expressed in ML as defined in the legend.

the SiO_2 bulk, (i.e., dark gray region in Figure 1) consists of Si^{1+}, Si^{2+}, and Si^{3+} suboxide components. Generally, the Si^{1+}, Si^{2+}, Si^{3+}, and Si^{4+} components are supposed to arise from interfacial silicon atoms, which bind to one, two, three, and four nearest-neighbor oxygen atoms, respectively.[16,17] Silicon atoms that connect to four oxygen atoms (Si^{4+}) are the unique members of the silicon dioxide SiO_2 phase, although some overcoordinated and undercoordinated Si atoms can be found in this region as well.

Figure 1 clearly shows how the growth temperature, the incident oxygen species, and its initial kinetic energy affect the oxygenated silicon thickness. The change in oxygenated silicon thickness as a function of incident energy is smaller in the case of molecular oxidation than for atomic oxidation, due to the immediate breakup upon collision of the molecules. Indeed, as the molecules are given the same initial kinetic energy as the atoms, the individual atoms obtained after dissociation have less momentum and hence a lower velocity. Therefore, oxygen molecules do not penetrate as deep in the surface as the oxygen atoms. Furthermore, in all cases, the growth temperature significantly affects the interface thickness, rather than the thickness of the SiO_2 (silica layer). Note that the interface thickness is limited in all cases up to 700 K due to the activation energy barrier associated with the penetration of successive Si layers by the impinging oxygen species. However, above this temperature, the interface atoms can surmount this energy barrier, which results in a higher diffusivity. Therefore, the temperature of 700 K can be regarded as the transition temperature between the two different growth mechanisms during hyperthermal oxidation, as will be explained in section 3. This result is in close agreement with experimental evidence for thermal oxidation. Indeed, it was found that the interstitial neutral oxygen atoms and molecules become mobile above 200 °C (~500 K) and 400 °C (~700 K), respectively.[15]

For a given incident species, the thickness of the oxide layer depends on two factors, namely, the incident energy and the growth temperature. Our results indicate that at temperatures below 700 K, both the final thickness of the silica layer and the growth mechanism depend mostly on the incident energy. Indeed, the oxygenated silicon and ultrathin silica thickness can be easily controlled by the particle impact energy at low temperature. At higher temperatures, the thickness and the growth mechanism strongly depend on the growth temperature as well. Indeed, in this case, the mobility of the penetrated oxygen atoms increases significantly. As mentioned above, in hyperthermal oxidation, all incident molecules dissociate to individual atoms due to the (relatively) high impact energy. Therefore, the mobility of the molecules in the oxygenated silicon cannot be analyzed.

Analysis of the interface region, which is located between the silica (SiO_2) and crystalline Si phases, by means of the number of suboxide components (Si^{1+}, Si^{2+}, and Si^{3+}) after oxidation by 32 ML of oxygen atoms (see Figure 2a) clearly shows the two types of interfaces, i.e., at temperatures below and above the transition temperature of 700 K. Below the transition temperature (i.e., 100−500 K), a very thin interface is formed of about 5 Å (cf. Figure 1). In this interface, the number of these suboxide components is less than 1 ML, as is clear from Figure 2a. Above this transition temperature (i.e., 900−1300 K), however, their number drastically increases with increasing growth temperature. This means that mobile oxygen atoms continue to penetrate deeper into the silicon. Especially, the number of the Si^{1+} species dominates in the interface region due to the high diffusivity of the oxygen atoms.

In Figure 2b, the appearance of silica and its growth behavior at different temperatures is presented by means of the number of Si^{4+} components, expressed in number of ML, plotted after different values of ML impacts, as indicated by the legend. At temperatures below 700 K, the first silica layer appears after 4 ML, whereas above this temperature, no silica layer is observed yet. Subsequently, after 8 ML, the number of Si^{4+} components is much higher at low temperature than at high temperature, indicating that the initial growth of the silica layer occurs much faster at low than at high temperature. However, after 32 ML, the number of Si^{4+} components is almost the same at all temperatures. This indicates that the silica layer now grows faster at higher temperature, but its nucleation started later. The rapid growth of the silica layers can be understood from the growth mechanism as will be outlined below.

Indeed, in the traditional thermal oxidation regime, the onset of silicon oxidation is characterized by an incubation period, i.e., the oxide thickness remains constant during this period, and is equal to the initial native-oxide thickness. The duration of this incubation period decreases with increasing temperature.[44] However, our results presented in Figure 2 show that the mechanism is different in the case of hyperthermal oxidation. Therefore, in the following section, we study the onset of the hyperthermal Si oxidation process in more detail.

Onset of Hyperthermal Si Oxidation. In the hyperthermal oxidation process, our results show that the initial oxidation stage can be divided in a first direct oxidation stage and a second relatively slow one. These two stages are governed by the initial kinetic energy of the impacting species and the growth temperature, respectively. The oxidation onset is characterized by direct insertion of incident oxygen species in

dx.doi.org/10.1021/jp300506g | J. Phys. Chem. C 2012, 116, 8649−8656

the Si crystal. Indeed, direct insertion of oxygen atoms into the Si subsurface layers occurs during the initial oxidation stage in the hyperthermal oxidation process, which is not observed in thermal oxidation. We explain this as follows. In the hyperthermal energy regime, the incident atoms having kinetic energies in the range E_0 = 1.0−5.0 eV, in our case, can surmount the energy barriers of the first and second subsurface layers,[1,2,9] which are estimated to be about 1.0 and 2.4 eV, respectively.[18] In other words, oxygen species can be incorporated directly in the silicon substrate. Such oxidation behavior near room temperature was also studied by ellipsometry and synchrotron radiation photoemission spectroscopy.[1,5,45] Formation and growth of the oxygenated silicon during this direct oxidation stage can be easily understood by observing the variation of the silicon suboxide components.

Figure 3 shows the evolution of Si suboxide components at various surface temperatures during the first 4 ML of oxygen

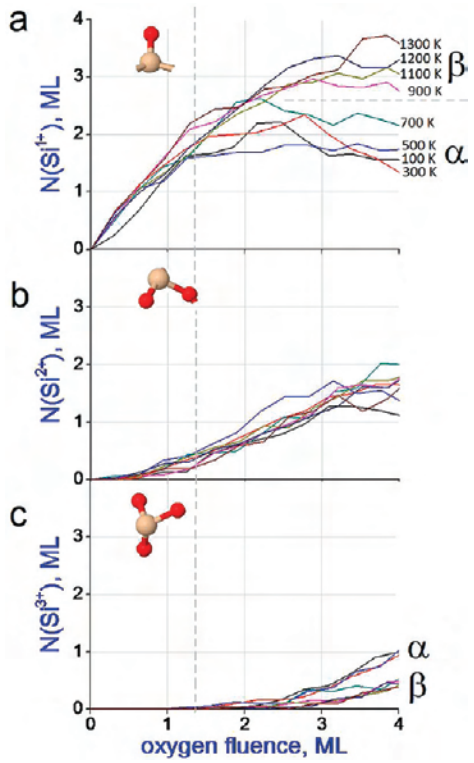

Figure 3. Analysis of the initial oxidation stage (i.e., up to 4 ML impacts) by means of the Si suboxide components: Si^{1+}, Si^{2+}, and Si^{3+} are silicon atoms, which bind to one, two, and three nearest-neighbor oxygen atoms, respectively. Here, α and β indicate the two groups of curves related to the low (100−500 K) and high (900−1300 K) temperature cases, respectively.

impacts (shown for a kinetic energy of 5 eV). In this initial oxidation stage, only the formation of substoichiometric (SiO_x) oxide layers is observed, i.e., the silicon dioxide (SiO_2) layer does not appear in this period (see also Figure 2b above). As shown in Figure 3a, the Si^{1+} species (i.e., Si atoms connected to a single O-atom) dominates in this stage. The Si^{1+} density increases linearly up to about 1.5 ML impacts, due to direct incorporation of the impinging hyperthermal oxygen atoms. In this short period (i.e., direct oxidation stage), it is the incident energy that determines the Si^{1+} density, rather than the growth temperature. Our results predict that the duration of this stage depends on the initial energy and type of the incident oxygen species, as explained below.

As mentioned above, the chemisorption process of the impinging oxygen molecules is found to be dissociative in this stage. Therefore, the penetrating species are exclusively O atoms, also in the case of O_2 molecule impact. Analysis of the direct penetration of atoms after impact on the Si surface shows that the impinging oxygen atoms can penetrate the Si substrate up to a depth between the second (i.e., 2.4 Å from the surface) and the seventh (i.e., 9.0 Å from the surface) Si subsurface layer in this direct oxidation stage. Note that the final penetration depth per impact is found to be determined in the first picosecond and essentially remains constant afterward, thereby validating our impingment rate of 1 impact every 3 ps.

As stated in the beginning of this section, the initial oxidation stage can be divided in a first direct oxidation stage and a second relatively slow oxidation stage. The end of the first direct oxidation stage is indicated by the vertical dashed line as shown in Figure 3. At this moment, Si^{2+} is also found (Figure 3b), and its density continues to increase slightly in the second oxidation stage. At low temperatures, the O atoms cannot penetrate deeper into the crystal at the end of the direct oxidation stage, and the Si^{1+} gradually converts to Si^{2+} and Si^{3+}. This conversion from Si^{1+} to Si^{2+} and Si^{3+} characterizes the second oxidation stage. The Si^{3+} component appears only in this oxidation stage, and two groups of curves (indicated by α and β in Figure 3c) are found. Note that in the lower temperature range (i.e., curves indicated by α), the density of Si^{3+} suboxide species increases slightly faster than at higher temperatures (i.e., curves indicated by β). This means that at low temperature, the consecutive $Si^{1+} \rightarrow Si^{2+} \rightarrow Si^{3+} \rightarrow Si^{4+}$ conversion, i.e., the appearance of a new silica layer, occurs much faster than at high temperatures. Indeed, the penetrated O atoms cannot move deeper into the crystal due to the energy barrier, and the Si−Si bonds convert relatively fast to Si−O bonds in the oxygenated silicon region. As a result, the formed silica layer is found to be thicker at low temperature at the same oxidation stage (see Figure 2b). Furthermore, during the conversion, the most stable Si−O bonds appear near the surface, which can significantly affect the sticking rate of the incident oxygen species. In all impact cases, the density of the penetrated O atoms drastically decreases after the initial oxidation stage. This, of course, affects the thickness of the oxygenated silicon. At higher growth temperatures, however, oxygen atoms can penetrate deeper due to their higher diffusivity. As a result, the conversion of the Si^{1+} to Si^{2+} and Si^{3+} is slower. Therefore, the second group of curves (see Figure 3c) in Si^{3+} changes less than the first group of curves. Indeed, the relatively slow conversion of the Si suboxide components is caused by the diffusion of the interstitial oxygen atoms, allowing the oxygen to penetrate deeper into the silicon bulk due to the easy surmounting of the energy barrier in this higher temperature range. Also, because the conversion is slower, the interface region becomes much thicker at high temperature than at low temperature, as was indeed clear from Figure 1.

Finally, when one complete silica layer is formed, the initial oxidation period, which consists of a direct oxidation stage and a relatively slow one as mentioned above, ends. This corresponds to the addition of 4 ML of oxygen atoms. Because of the energy barriers, the penetrated atoms lose their kinetic energy rapidly, and further inward oxygen displacement is prevented (below the transition temperature region) or

dx.doi.org/10.1021/jp300506g | J. Phys. Chem. C 2012, 116, 8649−8656

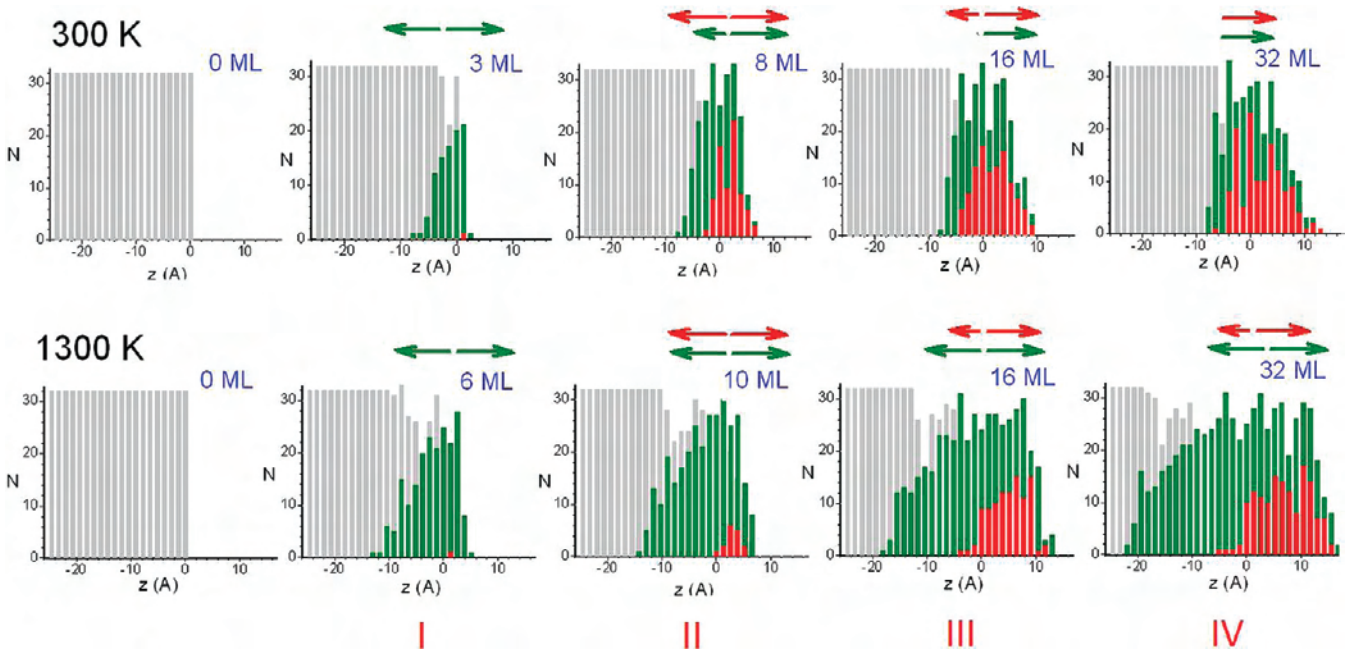

Figure 4. Growth behavior of oxidized silicon and ultrathin silica layers induced by 5 eV atomic oxygen at temperatures of 300 and 1300 K. The occurrence of pure Si, SiO_x ($x < 2$), and SiO_2 phases is indicated in the histograms by light gray bars, green bars, and red bars, respectively. Green and red arrows indicate the growth direction of the oxidized silicon and silica layers, respectively.

controlled by the growth temperature (above the transition temperature region). Therefore, we believe that the threshold temperature (see Figure 3a, dashed horizontal line) is an important factor in controlling the formation of the oxygenated silicon.

To conclude, the initial oxidation stage is indicative of some notable differences between the hyperthermal oxidation and traditional thermal oxidation, i.e., instead of an incubation period,[44] direct oxidation is observed with a specific duration that depends on the energy of the incident species. As this can change the growth mechanism of the oxide layer in the initial oxidation stage, we analyze the hyperthermal oxide growth mechanism in the next section.

Growth Mechanism of Oxide Layers in Hyperthermal Si Oxidation. As mentioned above, the silicon oxidation behavior is significantly different below and above the transition temperature. Here, we analyze the growth mechanism of the oxide layers in both cases. In Figure 4, the SiO_2 growth process on a $\{2 \times 1\}$ reconstructed Si(100) surface by oxygen atoms with an incident energy of 5 eV at 300 and 1300 K is presented. The oxidation progress is shown by suboxide histograms. Here, gray, green, and red bars describe the density distribution per depth of pure Si, oxygenated Si (i.e., SiO_x) species (with $x < 2$), and ultrathin silica (i.e., SiO_2) layers, respectively. The $z = 0$ Å position corresponds to the topmost layer of the original pristine Si lattice. Our calculations are based on the mass center position of Si layer planes[46] and show that the average thickness of each layer is equal to 1.296 Å, corresponding to the thickness of one-half oxide layer (i.e., the thickness of one oxide layer is 2.6 Å[5]). We analyzed the growth mechanism by comparing four specific stages (denoted as I, II, III, and IV in Figure 4) during the growth process at 300 and 1300 K.

In stage I, for both cases, the oxidized layers grow simultaneously inward and outward, normal to the surface; note that the green arrows indicate the growth direction of oxidized layers in Figure 4. In this stage, the number of the Si^{1+} component increases significantly, as was clear from Figure 3a. This corresponds to the initial oxidation stage, which was discussed in section 2. The appearance of an incipient silica layer indicates the end of stage I.

Stage II is indicated by the appearance and growth of the silica layer. At this stage, not only the oxidized layers but also the silica grows in two directions, i.e., inward and outward, at both temperatures (the red arrows indicate the growth direction of silica in Figure 4). Because of the relatively high activation energy barrier, however, the inward growth rate of the oxidized layer drops at low temperature. In that case, as mentioned in section 2, the $Si^{1+} \rightarrow Si^{2+} \rightarrow Si^{3+} \rightarrow Si^{4+}$ conversion is fast, and a new silica layer quickly forms and grows faster than at high temperature. As a result, the thickness of ultrathin SiO_2 obtained at low temperature is slightly higher than at high temperature, as was obvious from Figure 2b.

In stage III, the inward growth at low temperature is slowed down, especially for the oxidized layer but also for the silica layer, and the O atoms cannot penetrate in the crystal any further due to the associated activation energy barrier of the Si subsurface layers, which is in the order of 1 and 2.4 eV for the first and second Si subsurface layers, respectively.[18,19] However, at higher temperature, interstitial neutral oxygen atoms are still sufficiently mobile to surmount the activation energy barrier. In ref 15, a threshold temperature of 500 K for this process was suggested. Therefore, at higher temperature, both the inward and outward growth of the substoichiometric (SiO_x) and the stoichiometric (SiO_2) oxide layers still continues. However, the inward growth of the silica layer slows down, in a similar way as at low temperature.

In stage IV, i.e., the final stage, the inward growth becomes negligible at low temperature. Therefore, in this stage, only the outward growth of the oxidized silicon and silica phases continues. Our earlier study on the growth mechanism at room temperature[6] showed that, during the entire oxidation process (150 ML), the penetrated oxygen atoms can move only up to a

dx.doi.org/10.1021/jp300506g | J. Phys. Chem. C 2012, 116, 8649−8656

certain limit depth, which is about 10 Å from the top of the surface of the pristine crystalline Si. The limit of the oxidized depth is equal to the maximum penetration depth of the oxygen atoms, and it determines the maximum number of silicon atoms that may contribute to the formation of the oxygenated silicon layers. The limit depth is found to be nearly constant after stage IV, and it depends on both the kinetic energy and the type of incident oxygen species. The maximum penetration depth was found to be 5 and 9 Å for the atomic oxidation case with kinetic energies of 1 and 5 eV, respectively. In the case of oxidation by molecular oxygen, the limit depths were slightly lower than in the atomic case and the values were equal to 4 and 8 Å for kinetic energies of 1 and 5 eV, respectively. The limit depths are also close to the values of our previous calculations.[47]

At high temperature, however, both the oxidized silicon and silica layers continue to grow in both directions (i.e., inward and outward), although the inward silica growth rate drops. In that case, the interface, which consists of the Si^{1+}, Si^{2+}, and Si^{3+} species, is significantly thicker than at low temperature, as was also observed in Figure 1. The oxide thickness attains its maximum value when also the outward growth of the silica stops (not shown in Figure 4).

Study of the outward and inward displacement of silicon and oxygen species in the oxide growth process also allows a further understanding of the growth mechanism. In Figure 5 the

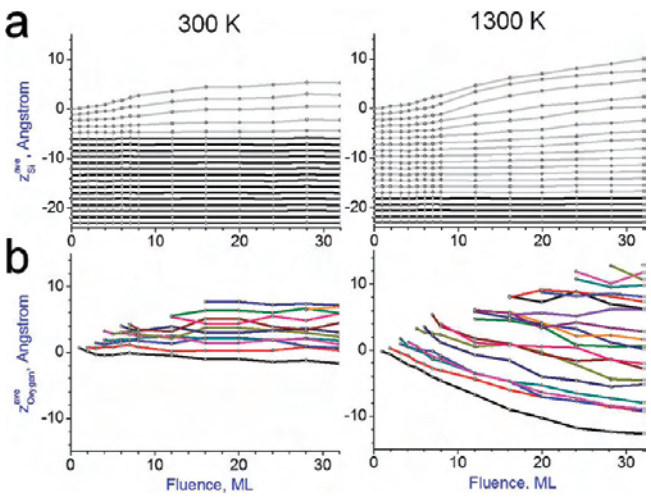

Figure 5. Evolution of (a) the growth of oxygenated Si layers, as shown by the average z coordinate of the silicon atoms per atomic layer and (b) the inward diffusion depth of penetrated oxygen during hyperthermal oxidation by oxygen atoms of 5 eV, at temperatures of 300 and 1300 K, respectively. Here, z = 0 Å corresponds to the topmost layer of the original pristine Si lattice. The black curves in panel a indicate the pure Si layers, whereas the gray curves indicate the Si atoms in the oxidized layers. The curves with different colors in panel b just represent different oxygen layers but have no further specific meaning.

evolution of the Si and O layers is shown as a function of oxygen fluence, during the oxidation at 300 and 1300 K. As mentioned above, z = 0 Å corresponds to the topmost layer of the original pristine Si lattice in both cases. In Figure 5a, each line corresponds to the average z coordinate of the Si atoms (belonging to the pristine substrate layer) as a function of the oxidation progress, expressed in number of added ML of oxygen. The simulated Si crystal consists of 20 layers, with an initial interlayer separation of about 1.3 Å.

We interpret the results as follows. At the very beginning of the oxidation process, the lines indicate that the upper surface and subsurface layers remain in place. In this short period (direct oxidation stage), some oxygen atoms can penetrate up to the limit depth of about 9 Å in the low temperature (300 K) case.[47] During the growth process, the top layers expand and the distance between the layers doubles relative to the initial separation (see light gray lines in Figure 5a), corresponding to one oxide layer.[5] By comparing both temperatures, it can be seen that the thickness of the formed silica layer is almost the same in both cases for the same oxidation time, but a thicker oxygenated silicon layer is obtained at high temperature (as was also obvious from Figure 1). The silica structure obtained at higher temperatures contains some Si−Si bonds, i.e., under-coordinated Si atoms, which is explained by the relatively slow conversion of the Si suboxide components. Therefore, the distance between the lines (layers) is different from the interlayer distance at lower temperature. Furthermore, we did not observe the outward displacement of any Si atom that is not connected to oxygen atoms. As mentioned in the introduction, according to the reactive layer model,[29] silicon atoms should diffuse through the thin reactive layer and react with oxygen on the top of this layer, forming the SiO_2 phase, which is not the case in our simulations. Therefore, this model cannot describe the growth behavior in hyperthermal oxidation.

In Figure 5b, each line corresponds to the average z coordinate of 32 penetrated oxygen atoms during oxidation. Positive z values indicate oxygen atoms adsorbed on top of the Si surface, whereas negative z values represent penetrated oxygen atoms due to inward diffusion during the oxidation process. Note that, due to the increasing activation energy, inward oxygen diffusion is observed only at temperatures above the transition temperature. At low temperature, inward oxygen growth is inhibited by the associated energy barrier. Indeed, in hyperthermal oxidation in this temperature region, the kinetic energy of the incident oxygen atoms is the dominant factor, rather than the growth temperature. In contrast, in the oxidation process at high temperature, oxygen atoms are continuously being displaced due to their high diffusivity. However, we did not observe the oxidation by oxygen diffusion through oxidized layers. Hence, also the Deal−Grove model[21] does not describe the hyperthermal oxidation mechanism as observed in our simulations.

Hence, our growth mechanism predicts that, when the temperature is below the transition temperature (i.e., $T < T_{transition}$), the oxide thickness depends on the kinetic energy of the incident oxygen species. However, in the case $T > T_{transition}$, the oxide thickness depends on both the incident energy and the growth temperature. Note that these predictions are not observed nor expected in the traditional thermal oxidation process.

Analysis of the Oxygenated Si Structure during Oxidation. Figure 6 shows the oxygen content and the energy gain of the oxygenated + nonoxygenated system as a function of the oxygen atom fluence at 5 eV. As can be seen in Figure 6b from the calculated system energy gain, the oxygenated silicon is energetically more stable than pure silicon. This stabilization occurs due to the formation of the Si−O bonds. Moreover, the total energy of the oxygenated silicon bulk strongly depends on the temperature, i.e., the system appears to become more stable with increasing growth temperature at this impact energy. It was found that the energy gain depends also on the incident

dx.doi.org/10.1021/jp300506g | J. Phys. Chem. C 2012, 116, 8649−8656

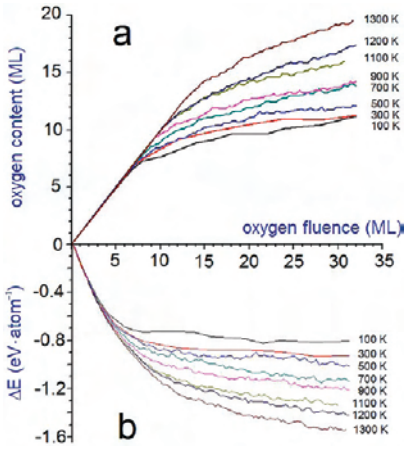

Figure 6. Oxygen content during hyperthermal oxidation of the {2 × 1} reconstructed Si(100) surface at various temperatures (a) and variation of the total energy of the oxygenated system (b) as a function of fluence, for an atomic oxygen beam with 5 eV kinetic energy.

energy and type of the oxygen species, i.e., the energy gain is higher in atomic oxidation and for higher initial impact energy.

Our previous results[6] predicted that the silica thickness also strongly depends on the type and initial energy of the incident oxygen species at room temperature. As mentioned above, it was found that the ultrathin silica films formed by this hyperthermal oxidation process can be divided in a pure silica bulk region and a silica surface region during oxidation. The roughness of the silica surface is rather high, and its mass density is lower than that of the pure silica bulk. Such a rough surface is found at all temperatures (see also Figure 1). Indeed, the surface roughness is also related to the incident energy rather than to the growth temperature.

In Figure 7, both the total and partial O−O radial distribution functions (RDFs) are shown for the structures

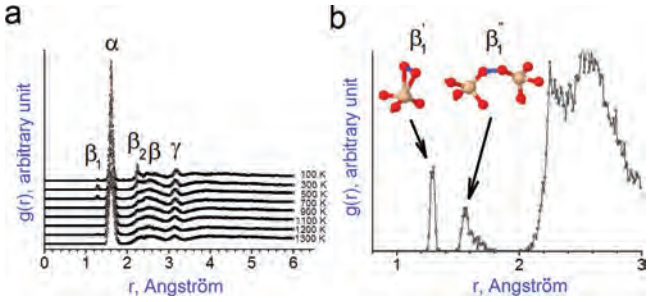

Figure 7. (a) Total radial distribution functions (RDFs) of the SiO_2 bulk silica structures during hyperthermal oxidation, for an atomic oxygen beam with 3 eV kinetic energy at different growth temperatures, and (b) partial distribution function of the O−O distance at 300 K, showing also two types of oxygen peroxyl bridge bond in silica. The symbols α, β, β_1 (β'_1, β''_1), β_2, and γ denote Si−O, O−O, O peroxyl (first type at 1.3 Å and second type at 1.6 Å), and nonbonded O−O and Si−Si bonds, respectively.

grown by 3 eV atomic impacts, for all temperatures. Very similar RDFs are obtained for impact energies of 1 and 5 eV (not shown). In Figure 7a, analysis of the silica structure by means of the RDF shows that the Si−O (α peak), O−O (β peak), and Si−Si (γ peak) bonds are located at 1.6 Å, 2.5 Å, and 3.2 Å, respectively. These values agree with both experimental values and other MD calculations.[38,48,49] Moreover, only the α peak is sharp, whereas the other peaks are rather weak, indicating that the obtained structures are amorphous. However, at low temperature, some unexpected O−O nonbonded neighbors (β_2 peak) are found with a distance of 2.25 Å, close to the β peak. We believe that this peak is caused by stress near the interface. The β_2 peak also depends on the growth temperature, i.e., increasing the growth temperature significantly decreases these O−O interactions in the tetrahedral silicon structure. Also, some unexpected peaks in the RDF analysis indicate some intrinsic defects, i.e., peroxyl bridges (see β'_1 and β''_1 in Figure 7b), 3-fold oxygen, as well as over- and undercoordinated silicon atoms can be found in the silica structure during oxidation. The existence of peroxyl bridges and 3-fold bond configurations in amorphous SiO_2 has already been suggested on the basis of some experimental and first-principles calculations.[15,50−52] Indeed, it was suggested that the peroxyl bridge configuration is energetically stable. Our results also show that such peroxyl linkages occur more in the silica induced by atomic oxidation than by molecular oxidation at temperatures below the transition temperature, although their number is small. The results also show that the total number of oxygen peroxyl bridges significantly decreases with increasing growth temperature.

Finally, the ability to accurately control the growth of ultrathin α-SiO_2 and its interface thickness increases with decreasing growth temperature. As demonstrated in the previous sections, the interface thickness strongly depends on the growth temperature, due to the increasing mobility and diffusivity of the penetrated oxygen atoms at higher temperatures. We therefore believe that the transition temperature is one of the key factors in controlling the thickness of the ultrathin silica with an abrupt interface. Indeed, the thickness of the ultrathin silica is most easily controlled by the incident energy and type of the incident oxygen species at temperatures below the transition temperature (i.e., at temperatures below 500−700 K).[6]

SUMMARY AND CONCLUSIONS

The temperature dependence of hyperthermal oxidation of Si(100) {2 × 1} surfaces by oxygen atoms and molecules was analyzed by reactive molecular dynamics simulations. A transition temperature of about 700 K was found: below this temperature, the oxide thickness only depends on the impact energy of the impinging species. Above this temperature, the oxide thickness depends on both the impact energy and the surface temperature. More specifically, the oxide thickness increases with increasing temperature. This is caused by the enhanced diffusivity of the oxygen atoms with increasing temperature as well as the activation barrier for oxygen penetration in the silicon crystal. Furthermore, the initial oxidation stage in hyperthermal oxidation shows some notable differences from the traditional thermal oxidation: instead of an incubation period, an initial stage of direct oxidation with a specific duration is observed. This changes the growth mechanism of the oxide layer in the initial oxidation stage. Two growth mechanisms of the bulk silica and interface region were found, corresponding to temperatures below and above the transition temperature. Where possible, we validated our results with experimental and ab initio data, and good agreement was obtained. These results are of importance for the fabrication of silica-based devices in the micro- and nanoelectronics industry and open up a new route for silica growth by hyperthermal oxidation.

dx.doi.org/10.1021/jp300506g | J. Phys. Chem. C 2012, 116, 8649−8656

AUTHOR INFORMATION

Notes

The authors declare no competing financial interest.

ACKNOWLEDGMENTS

U.K. acknowledges IMEC for financial support. E.C.N. acknowledges the FWO-Flanders (Fund for Scientific Research-Flanders) for financial support. A.C.T.v.D. acknowledges funding from the Air Force Office of Scientific Research (AFOSR) under Grant No. FA9550-10-1-0563. We also gratefully acknowledge financial support from the Prime Minister's Office through IAP VI. This work was carried out using the Turing HPC infrastructure at the CalcUA core facility of the Universiteit Antwerpen (UA), a division of the Flemish Supercomputer Center VSC, funded by the Hercules Foundation, the Flemish Government (department EWI), and the UA. Finally, we also thank Professor A. Bogaerts for the useful discussions.

REFERENCES

(1) Tagawa, M.; Yokota, K.; Tsumamoto, S.; Sogo, C.; Yoshigoe, A.; Teraoka, Y. *Appl. Phys. Lett.* **2007**, *91*, 033504.
(2) Tagawa, M.; Yokota, K.; Ohmae, N.; Kinoshita, H.; Umeno, M. *Jpn. J. Appl. Phys., Part 1* **2001**, *40*, 6152.
(3) Tagawa, M.; Sogo, C.; Yokota, K.; Yoshigoe, A.; Teraoka, Y.; Shimura, T. *Appl. Phys. Lett.* **2006**, *88*, 133512.
(4) Teraoka, Y.; Yoshigoe, A. *Surf. Sci.* **2002**, *507*−*510*, 797−802.
(5) Yoshigoe, A.; Teraoka, Y. *Surf. Sci.* **2003**, *532*−*535*, 690−697.
(6) Khalilov, U.; Neyts, E.; Pourtois, G.; van Duin, A. C. T. *J. Phys. Chem. C* **2011**, *115*, 24839−24848.
(7) Murad, E. *J. Spacecr. Rockets* **1996**, *33*, 131.
(8) Tzvetkov, T.; Qin, X.; Jacobs, D. C. *Phys. Rev. B* **2003**, *67*, 075418.
(9) Kisa, M.; Minton, T. K.; Yang, J. C. *J. Appl. Phys.* **2005**, *97*, 23520.
(10) Okada, M. *J. Phys.: Condens. Matter* **2010**, *22*, 263003 and references therein.
(11) Ferguson, B. A.; Reeves, C. T.; Mullins, C. B. *J. Chem. Phys.* **1999**, *110*, 11574−11577.
(12) Hamann, D. R. J. *Phys. Rev. Lett.* **1998**, *81*, 3447−3450.
(13) Miyake, T.; Soeki, S.; Kato, H.; Nakamura, T.; Namiki, A.; Kamba, H.; Suzaki, T. *Phys. Rev. B* **1990**, *42*, 11801−11807.
(14) Orellana, W.; Antonio, J. R.; da Silva; Fazzio, A. J. *Phys. Rev. Lett.* **2003**, *90*, 016103.
(15) Kajihara, K.; Miura, T.; Kamioka, H.; Aiba, A.; Uramoto, M.; Morimoto, Y.; Hirano, M.; Skuja, L.; Hosono, H. *J. Non-Cryst. Solids* **2008**, *354*, 224−232 and references therein.
(16) Oh, J. H.; Nakamura, K.; Ono, K.; Oshima, M.; Hirashita, N.; Niwa, M.; Toriumi, A.; Kakizaki, A. *J. Electron Spectrosc. Relat. Phenom.* **2001**, *114*−*116*, 395−399.
(17) Choi, C. H.; Liu, D.; Evans, J. W.; Gordon, M. S. *J. Am. Chem. Soc.* **2002**, *124*, 8730−8740.
(18) Kato, K.; Uda, T.; Terakura, K. *Phys. Rev. Lett.* **1998**, *80*, 2000.
(19) Watanabe, H.; Kato, K.; Uda, T.; Fujita, K.; Ichikawa, M.; Kawamura, T.; Terakura, K. *Phys. Rev. Lett.* **1998**, *80*, 345−348.
(20) Bongiorno, A.; Pasquarello, A. *J. Mater. Sci* **2005**, *40*, 3047−3050.
(21) Deal, B. E.; Grove, A. S. *J. Appl. Phys.* **1965**, *36*, 3770−3778.
(22) Gusev, E. P.; Lu, H. C.; Gustafsson, T.; Garfunkel, R. *Phys. Rev. B* **1995**, *52*, 1759−1770 and references therein.
(23) Bongiorno, A. *Simulation of Atomistic Processes during Silicon Oxidation*. Ph.D. Thesis, Lausanne, EPFL, 2003, and references therein.
(24) Massoud, H. Z.; Plummer, J. D.; Irene, E. A. *J. Electrochem. Soc.* **1985**, *132*, 1745.
(25) Cerofolini, G. F.; Mascolo, D.; Vlad, M. O. *J. Appl. Phys.* **2006**, *100*, 054308.
(26) Elovich, S. J. *Proceedings of the Second International Congress on Surface Activity*; Schulman, J. H., Ed.; Academic Press, Inc: New York, 1959; Vol. *11*, p 253.
(27) McLintock, I. S. *Nature* **1967**, *216*, 1204−1205.
(28) Atkinson, R. J.; Hingston, F. J.; Posner, A. M.; Quirk, J. P. *Nature* **1970**, *226*, 148−149.
(29) Stoneham, A. M.; Grovenor, C. R. M.; Carezzo, A. *Philos. Mag.* **1985**, *55*, 201−10.
(30) Uematsu, M.; Kageshima, H.; Shiraishi, K. *Comput. Mater. Sci.* **2002**, *24*, 229−234.
(31) van Duin, A. C. T.; Dasgupta, S.; Lorant, F.; Goddart, W. A., III. *J. Phys. Chem. A* **2001**, *105*, 9396−9409.
(32) Abell, G. C. *Phys. Rev. B* **1985**, *31*, 6184−6196.
(33) Mortier, W. J.; Ghosh, S. K.; Shankar, S. *J. Am. Chem. Soc.* **1986**, *108*, 4315−4320.
(34) van Duin, A. C. T.; Baas, J. M. A.; van de Graaf, B. *J. Chem. Soc., Faraday Trans.* **1994**, *90*, 2881−2895.
(35) van Duin, A. C. T.; Strachan, A.; Stewman, S.; Zhang, Q.; Xu, X.; Goddard, W. A., III. *J. Phys. Chem. A* **2003**, *107*, 3803−3811.
(36) Buehler, M. J.; van Duin, A. C. T.; Goddard, W. A. *Phys. Rev. Let.* **2006**, *96*, 095505.
(37) Ning, N.; Calvo, F.; van Duin, A. C. T.; Wales, D. J.; Vach, H. *J. Phys. Chem. C* **2009**, *113*, 518−523.
(38) Fogarty, J. C.; Aktulga, H. M.; Grama, A. Y.; van Duin, A. C. T.; Pandit, S. *J. Chem. Phys.* **2010**, *132*, 174704.
(39) Neyts, E. C.; Shibuta, Y.; van Duin, A. C. T.; Bogaerts, A. *ACS Nano* **2010**, *4*, 6665−6672.
(40) Neyts, E. C.; van Duin, A. C. T.; Bogaerts, A. *J. Am. Chem. Soc.* **2011**, *133*, 17225−17231.
(41) Valentini, P.; Schwartzentruber, T. E.; Cozmuta, I. *J. Chem. Phys.* **2010**, *133*, 084703.
(42) Mueller, J. E.; van Duin, A. C. T.; Goddard, W. A., III. *J. Phys. Chem. C* **2010**, *114*, 5675−5685.
(43) Berendsen, H. J. C.; Postma, J. P. M.; van Gunsteren, W. F.; DiNola, A.; Haak, J. R. *J. Chem. Phys.* **1984**, *81* (8), 3684−3690.
(44) Kageshima, H.; Shiraishi, K. *Phys. Rev. Lett.* **1998**, *81*, 5936−5939.
(45) Massoud, H. Z. *Solid-State Electron.* **1997**, *41*, 929−934.
(46) Ganster, P.; Treglia, G.; Saul, A. *Phys. Rev. B* **2010**, *81*, 045315.
(47) Neyts, E.; Khalilov, U.; Pourtois, G.; van Duin, A. C. T. *J. Phys. Chem. C* **2011**, *115*, 4818−4823.
(48) Pasquarello, A.; Hybertsen, M.; Car, R. *Appl. Surf. Sci.* **1996**, *104/105*, 317−322.
(49) Mozzi, R. L.; Warren, B. E. *J. Appl. Crystallogr.* **1969**, *2*, 164−172.
(50) Ng, K.-O.; Vanderbilt, D. *Phys. Rev. B* **1999**, *59*, 10132−10137.
(51) Stoneham, A. M.; Szymanski, M. A.; Shluger, A. L. *Phys. Rev. B* **2001**, *63*, 221304−07.
(52) Bakos, T.; Rashkeev, S. N.; Pantelides, S. T. *Phys. Rev. Lett.* **2002**, *88* (5), 055508.